Structural aging of crystals of hard-sphere colloids

V. C. Martelozzo, A. B. Schofield, W. C. K. Poon, and P. N. Pusey
Department of Physics and Astronomy, The University of Edinburgh, Mayfield Road, Edinburgh, EH9 3JZ, Scotland, United Kingdom
(Received 28 November 2001; revised manuscript received 24 June 2002; published 27 August 2002)

We report a detailed experimental study of the aging of the (initial) random hexagonal close-packed (rhcp) crystals formed in suspensions of hard-sphere colloids near the melting point. By suspending the same colloidal particles in two different mixtures of solvents we are able to tune the strength of the gravitational forces acting on the particles. The crystal structure is deduced from diffraction patterns measured by the light scattering equivalent of powder x-ray crystallography. A spontaneous aging of the structure is observed over long periods of time, consisting of a fraction of pure face-centered cubic (fcc) crystals growing at the expense of the randomly stacked crystallites. The rate of growth of the new crystals is small and consistent with the predictions by Pronk and Frenkel [13]. Gravity is also revealed to affect the crystals and favor fcc order but through a slow gradual rearrangement of the random stacking. An important new observation is that small mechanical perturbations can strongly affect the structure of the colloidal crystals, promoting fcc growth and interfering with the spontaneous aging process. Previous experimental results are also discussed in the light of these new findings.

DOI: 10.1103/PhysRevE.66.021408 PACS number(s): 82.70.Dd, 61.72.Nn, 81.40.−z

I. INTRODUCTION

Hard spheres in thermally-induced motion constitute a simple and important model of condensed matter in both equilibrium and nonequilibrium states. Despite the lack of either long-range interactions or attractions, such a system exhibits a first-order phase transition from a fluid phase to a crystal phase upon increasing concentration [1,2]. This freezing transition is driven by entropy and occurs at a concentration where the decrease in the global (or configurational) entropy of the system is more than offset by the increase in the local (or free-volume) entropy. Ever since the first simulations of the late 1950s [1,2], hard-sphere freezing has been studied extensively, both theoretically and experimentally. While theoretical (computer simulation) studies of the stable structure of the hard-sphere crystal now appear to have reached definite conclusions (below), the experimental situation remains ambiguous.

The structure in which equal-sized spheres can be arranged so as to minimize the volume they occupy is a stacking of close-packed hexagonal layers [3–5]. As we will see in more detail in Sec. III, there are many ways in which this can be done, leading to many different structures. The two simplest structures are face-centered cubic, fcc (an $\ldots ABCABC \ldots$ stacking, Sec. III) and hexagonal close-packed, hcp (an $\ldots ABABAB \ldots$ stacking). The free energy differences between the different hard-sphere crystals at fixed volume are due only to differences in entropy, since the energy is the same for all allowed configurations. The question of which crystalline stacking of hard spheres near close packing has the highest entropy was first tackled numerically back in the late 1960s [6–8], looking only at the fcc and hcp stackings. The entropies were obtained by integration of the pressure, calculated from molecular dynamics simulations. However, these early studies were not accurate enough to detect any entropy difference between the two structures. A decade later, Frenkel and Ladd [9] used a new Monte Carlo method to compute the free energy of the two structures and found an entropy difference $\Delta S = S_{fcc} - S_{hcp}$, per sphere, situated in the range $-0.001 < \Delta S < 0.002$, in units of k_B, indeed very small but still not precise enough to identify the stable structure. Other studies also took place around the same time using density functional theory but the results were also inconclusive: Colot and Baus [10] found that the free energy difference was too small to be evaluated, while Iglói [11] found that fcc was slightly more stable than hcp but with a difference of the same magnitude as the error associated with the calculations. Only very recently have new computer simulation techniques, implementations of the so-called multicanonical Monte Carlo method, allowed resolution of the very small entropy differences involved [12–15]. These studies find that fcc is entropically favored over hcp, with an entropy difference $\Delta S \approx 10^{-3} k_B$ per sphere and an uncertainty in ΔS down to as low as $10^{-5} k_B$. In the thermodynamic limit (a crystal of infinite size), the fcc structure has also been shown to be more stable than any of all other possible stackings [14].

Experimentally, hard spheres can be approximated by spherical colloidal particles, suspended in a liquid, with repulsive interactions whose ranges are very short compared to the particle radius. Deviations from ideal hard spheres are due to polydispersity (a distribution of size) and to interactions. Polydispersity can usually be minimized to ≈ 3–5%. The van der Waals attraction can also be reduced by matching the dielectric constants, or refractive indices, of the spheres and the suspension medium. Since the free energy differences between the different stackings are very small, one would expect the spontaneous generation of stacking faults during crystallization which could be slow to ''anneal out.'' Indeed, more than a decade ago, a study by Pusey *et al.* [16], based on light scattering measurements of powder diffraction patterns of crystals of nearly hard colloidal spheres, showed that, near to the melting concentration where crystallization is fast, the structure was essentially completely random hexagonal close-packed, rhcp (e.g., a stacking like $\ldots ABACBA \ldots$). However, the crystal structure was reported to tend towards fcc on increasing or decreasing the concentration of the samples, i.e., when crystallization is

slower. Further work by Chui [17,18] also seemed to indicate that with time, and at all concentrations, the crystals ripen into the fcc structure.

Experiments have also been carried out in microgravity [19,20]; under such conditions, the structure of the crystals was first reported to remain completely random hexagonal close-packed and, by comparison with the earlier ground-based studies, it was therefore concluded that gravitational stress promotes fcc. More recently, however, Cheng *et al.* [21] have reported data collected in the same microgravity conditions which show the gradual growth of fcc crystals. The authors thus concluded that fcc is the equilibrium-stable structure for hard-sphere crystals. Also quite recently, and indeed at the same time as the work to be described here, Kegel and Dhont [22] performed a slightly different study, looking at the ''aging'' of different initial stacking structures generated by applying various types of stress during crystal nucleation (in ''milligravity'' conditions, obtained by nearly matching the densities of the particles and the suspension medium). They found that ''faulted-twinned fcc'' crystals grew at the expense of the randomly stacked crystals. Furthermore when such crystals were generated initially, no change was found over a considerable time. They therefore concluded that the randomly stacked structure could not be the equilibrium structure of crystals of hard colloidal spheres but rather that the faulted-twinned fcc structure was the thermodynamically or kinetically stable structure.

The aim of the present work is to observe and study the expected aging of the initially random-stacked structure of colloidal hard-sphere crystals towards fcc ordering. We are interested in particular in observing the effect of gravity on the evolution of the crystal structure. This is done by studying in parallel two (nearly) hard-sphere suspensions, essentially identical in every respect except for the density difference between particles and suspension medium. Details about the colloidal suspensions used will be given in Sec. II A. The experimental setup used to probe the crystal structures consists of the light scattering equivalent of powder x-ray crystallography [16]; a brief description of the apparatus is outlined in Sec. II B. In Sec. III we then identify the different ways in which close packing may be generated, describe the corresponding scattering patterns expected and outline the model used to analyze the measured spectra. The results of our experiments and their analysis are presented in Sec. IV, where a qualitative assessment of the effect of gravity can be made immediately by direct comparison of the results obtained for the two systems. In this section, we also present rather unexpected results on the aging of the crystal structure when subjected to small mechanical perturbations. The perturbations are those imparted to the samples during (careful) transits between storage and measurement rig. Yet, as we will show, the effect on the crystal structure are significant. Finally, in Sec. V, we discuss our results, compare them with other recent experimental works as well as current theoretical predictions, and we briefly summarize our conclusions in Sec. VI.

II. EXPERIMENTAL DETAILS

A. System

The particles used in this study consisted of polymethylmethacrylate (PMMA) cores stabilized sterically by thin (10–15 nm thick) chemically grafted layers of poly-12-hydroxystearic acid (PHSA) chains [23]. They were dispersed in two different organic media. The first consisted of a mixture of cis-decahydronaphtalene (cis-decalin, $n=1.4810$) and 1,2,3,4-tetrahydronaphtalene (tetralin, $n=1.5410$) in proportions chosen so as to nearly match the refractive index of the particles [24]. The resulting density difference between particles and solvent in such samples was then found to be $\Delta\rho\approx 0.3\ \mathrm{g\,cm^{-3}}$. For the second, we nearly matched the density of the medium, as well as its refractive index, to that of the particles. This was achieved by mixing cis-decalin ($\rho=0.897\ \mathrm{g\,cm^{-3}}$) and bromocycloheptane ($n=1.5052$, $\rho=1.289\ \mathrm{g\,cm^{-3}}$), which bracket both the density and the refractive index of the particles [25]. However, the slight swelling of the particles by this medium ($\approx 1\%$ in radius) led to a larger density mismatch than projected, with $\Delta\rho\approx 5\times 10^{-2}\ \mathrm{g\,cm^{-3}}$.

The mean radius of the particles measured by light scattering and crystallography is 242 ± 0.5 nm in the nearly-index-matching mixture and 245 ± 0.5 nm in the other medium. The size polydispersity [(standard deviation of the particle size distribution)/mean], measured by two-color dynamic light scattering [26,27], on dilute suspensions in pure cis-decalin, is $5.0\pm 0.5\%$.

Previous works on similar systems have shown that the interaction between the particles is well approximated by that of hard spheres [24,25,28]. This was also verified here, by observing the position of the fluid-crystal transition [29]. Series of samples with concentrations spanning the transition were prepared from the same stock solution by removing/adding known masses of solvents. A similar phase behavior to that expected for hard spheres was observed upon increasing volume fraction ϕ (fraction of the total sample volume occupied by the particles). At low ϕ, samples remained in a single homogeneous phase, with a fluidlike arrangement of the particles. Above a given ϕ, crystal nucleation took place and coexisting colloidal fluid and crystalline phases were observed, the relative fraction of the sample occupied by the crystals increasing linearly with ϕ. Finally, at higher ϕ, the samples became completely filled with crystallites. The concentration at which crystallization first occured was identified with the hard-sphere freezing volume fraction $\phi_F=0.494$, as determined by computer simulations [30], and all other concentrations were scaled by that same factor to provide effective hard-sphere volume fractions (quoted here). The corresponding hard-sphere melting volume fraction, which was identified with the lowest concentration at which samples were fully crystalline, was then found to be $\phi=0.544$. This value is in very close agreement with that determined from computer simulations $\phi_M=0.545$ and supports the assumption of a steeply repulsive potential close to that of hard spheres.

B. Scattering setup

The structure of the crystals formed was studied using the light scattering equivalent of powder x-ray crystallography [16] (schematic shown in Fig. 1). The beam of a Kr^+-ion laser (tunable wavelength, 476.2–647.1 nm) was expanded

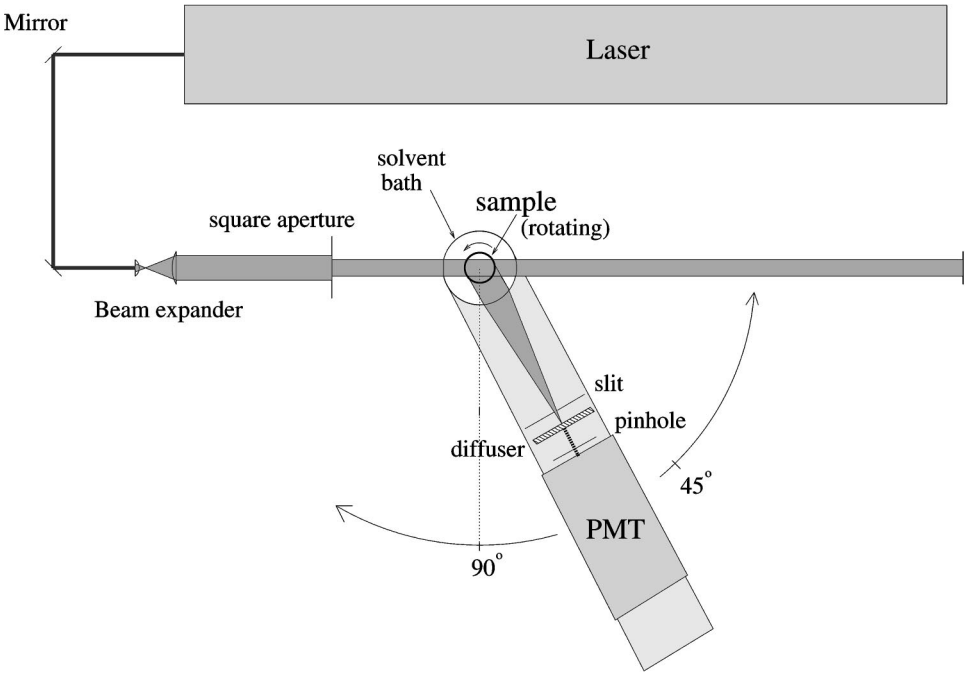

FIG. 1. Schematic of the static light scattering setup used to record the diffraction patterns of polycrystalline samples; see text for details.

and passed through an adjustable rectangular aperture in order to illuminate a chosen volume of the sample. The sample cell was held by a sample holder with three-dimensional vernier adjustments, positioned on the axis of a cylindrical bath. The bath, which has an optically flat window for the incident beam, was filled with an index-matching mixture of decalin and tetralin to eliminate refraction and any reflections at the glass/solvent interfaces. The index bath acted as a cylindrical lens, focusing parallel scattered radiation onto a vertical slit which preceded a diffuser and a photomultiplier-tube detector. These detection optics were mounted on a computer-controlled turntable allowing scans over scattering angles from 20° to 140° with a resolution of about 0.1°. The sample was contained in a cylindrical cuvette with a volume of 2.5 ml. The rectangular aperture was adjusted so as to illuminate a 2 mm slice, which enabled measurements to be performed at different heights. Each volume contained many randomly oriented crystallites, of the order of 10^{-1} mm in size; but, to optimize the averaging, the sample cell was steadily rotated about its vertical axis at an angular velocity ≈ 1 rev/s. Measurements were taken over a carefully selected range of wave vectors to include all the features required to define the structure and yet to minimize the duration of each run. At each angle, averages were taken over a period of 1 s (≈ 1 rev), making the duration of the runs ≈ 5 min at each height.

III. MODEL CALCULATION OF THE DIFFRACTION PATTERN

Close packing in 2D corresponds to the arrangement where each sphere is in contact with six others, i.e., an hexagonal plane lattice. 3D close-packed structures may be obtained by stacking these hexagonal layers in such a manner that the total volume occupied is minimized. This is achieved when one close-packed plane is placed on another close-packed plane so that three spheres in one plane are in contact with the same sphere in the other plane [3–5]. This means that each plane can adopt one of three lateral positions, usually designated *A*, *B* and *C*; taking *A* as the reference position, *B* is obtained by a translation $\boldsymbol{a}/3+2\boldsymbol{b}/3$ relative to *A*, and *C* by displacement $2\boldsymbol{a}/3+\boldsymbol{b}/3$, where $\boldsymbol{a}$ and $\boldsymbol{b}$ are the conventional hexagonal lattice vectors in the (close-packed) planes. The only requirement is that adjacent layers, n and $n+1$, have different lateral positions. Therefore many sequences of close-packed planes are possible. The close-packed structure derived from the infinite sequence $\ldots ABABAB \ldots$, which repeats every two layers, is the hexagonal close-packed (hcp) structure, and the sequence of planes $\ldots ABCABC \ldots$, which repeats every three layers, gives the face-centered-cubic (fcc) structure. Many other ''random-stacked'' sequences are also possible, such as $\ldots ABACAB \ldots$ and $\ldots ABABCA \ldots$, but $\ldots ABABAB \ldots$ and $\ldots ABCABC \ldots$ are the two simplest and the only two where every sphere in the crystal is related to every other by either the lattice translation or a symmetry operation. Nevertheless all sequences can be catalogued according to the degree of randomness in the stacking of the hexagonal planes. This is done by assigning a probability α that layers n and $n+2$ have different lateral positions. Therefore $\alpha=0$ corresponds to hcp, $\alpha=1$ to fcc, and a completely random sequence will have $\alpha=0.5$.

Calculation of the powder diffraction pattern comprises two steps, determination of the reciprocal space structure and orientational averaging. In the case of a single hexagonal plane with lattice parameter *a*, the reciprocal space is formed of a series of straight lines perpendicular to the plane and passing through the nodes of the plane lattice [31], i.e., hexagonally arranged with a spacing $a^*=4\pi/a\sqrt{3}$. For close-packed structures, or collections of N parallel hexagonal planes at a distance $c=a\sqrt{2/3}$ from each others (= half the conventionally used hcp lattice spacing), the reciprocal-space

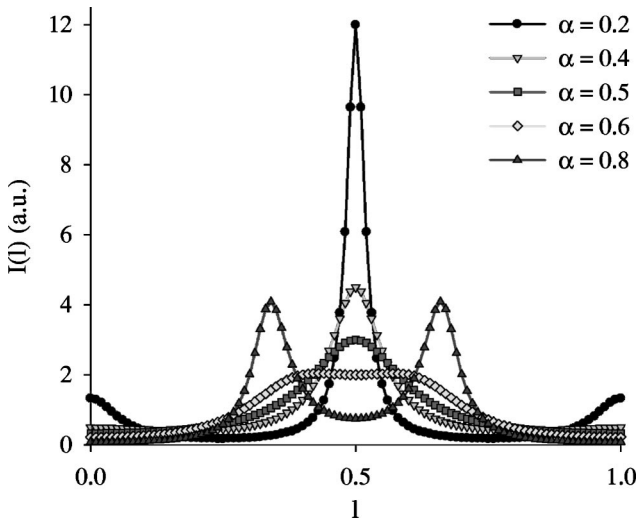

FIG. 2. $I(l)$ for different values of the stacking parameter α, corresponding to the expression derived in Ref. [31] [Eq. (17)], for rigid configurations of infinite stacks of 2D hcp layers whose stacking sequence is characterized by the (stacking) probability α.

unit vector along the lines has length $c^*=2\pi/c$ and the intensity distribution along the lines depends on the stacking sequence of the close-packed planes, hence α. In fact, the hk lines split into two categories which are differently affected by the exact stacking order. For lines such that $(h-k)/3$ is integral, the intensity distribution does not depend on the stacking order; it is concentrated at the points (h,k,l), where l is integral, corresponding to those Bragg reflections common to both (perfect) fcc and hcp structures. For the other lines, the intensity distribution depends on the stacking sequence. In the case of pure fcc structures, the intensity is concentrated at points where $l=m\pm 1/3$, with m integral, and for pure hcp structures, it consists of points at $l=m\pm 1/2$. For all the other sequences, $0<\alpha<1$, the intensity varies continuously along the hk lines in a manner determined by the stacking probability α. A completely random stacking ($\alpha=0.5$) gives an intensity profile continuously distributed along the lines, with maxima at $l=m\pm 1/2$ and minima at $l=m$ in a ratio of 9:1. Figure 2 shows various intensity distributions along the lines hk such that $(h-k)/3$ is not integral corresponding to structures with $0.2\lesssim\alpha\lesssim 0.8$ [32]. The finite size of the crystals also broadens the points into nodes and the lines into rods.

Orientational averaging can be achieved by constructing the Ewald sphere, as for single crystals, then by rotating it through all possible orientations around the origin of the reciprocal space, in order to account for all possible orientations of the crystallites. The corresponding set of scattering vectors therefore form concentric spheres around the origin and, for each magnitude of the scattering vector, the real-space powder intensity is proportional to the product of the fraction of the area of the sphere surface which intersects a feature in reciprocal space and the intensity of this feature [see, e.g., Fig. 1(d) of Ref. [16]]. For each scattering vector, one may first consider the (h,k) plane and check for intersections with the rods. Owing to the hexagonal symmetry of the arrangement, one need in fact only consider that portion of reciprocal space between the h axis and the line $h=k$, and multiply by the multiplicity factor to account for the full picture. For each of the features intersected, one may then determine the angular limits of the intersections above and below the plane, which are equivalent by symmetry. The real-space powder intensity can thereafter be calculated by integrating the intensity of the features over the corresponding angular range.

The two sets of rods give rise to qualitatively distinct contributions to the powder pattern. The discrete high-intensity nodes along the hk rods where $(h-k)/3$ is integral generate sharp Bragg peaks, while the continuous intensity distribution along the other rods results in broad bands of diffuse scattering. The width of the Bragg peaks is related to that of the nodes and is therefore inversely proportional to the size of the crystallites. The band of diffuse scattering around the main Bragg peak is not totally featureless; it comprises two main entities which reflect different properties of the crystals. The first arises from the initially very large area of intersection as the sphere first meets the rods; it consists of a prepeak, the width of which is related to the width of the rods, determined by the size of the crystals, and the height to the intensity along the rods, governed by the stacking probability α. The second part of this diffuse band, at higher wave vectors, consists of a much broader and featureless shoulder; its shape nonetheless varies sensitively with the intensity profile along the rods and provides a good measure of the stacking probablity α.

Theoretical powder patterns corresponding to close-packed structures with stacking probabilities ranging from $\alpha=0$ (hcp) to $\alpha=1$ (fcc) are plotted in Fig. 3. They were computed on the basis of the calculations by Loose and Ackerson [32], following the steps outlined above [33]. The value of the stacking probability has a considerable effect on the overall shape of the diffraction pattern and a narrow range of wave vectors centered around the main Bragg peak is sufficient to distinguish between the different structures. In this range of wave vectors, the pattern for $\alpha=0$, a regular hcp lattice, consists of four sharp Bragg peaks corresponding to the four sets of planes (100), (001), $(10\frac{1}{2})$ and (101). As the stacking probability α is increased, the peaks broaden and all gradually fade away except for the 001 peak which corresponds to the main reflections from the close-packed layers; for this reflection, the wave vector being perpendicular to the planes, the sequence of lateral positions is irrelevant. For a completely random stacking, $\alpha=0.5$, the powder spectrum has a very distinctive profile where the band of diffuse scattering around the main Bragg peak exhibits a relatively sharp prepeak and a broad ''hump'' at larger wave vectors. As α is increased further, the hump quickly vanishes and a new reflection appears at a slightly larger wave vector. This reflection is the $(10\frac{2}{3})$, corresponding to the $(200)_{fcc}$, which therefore sharpens upon increasing α. Finally for $\alpha=1$, a perfect fcc lattice, the pattern consists of two sharp Bragg peaks, from the sets of planes $(111)_{fcc}$ [corresponding to the (001) plane in the indexing used here and the (002) plane in the usual hcp indexing] and $(200)_{fcc}$.

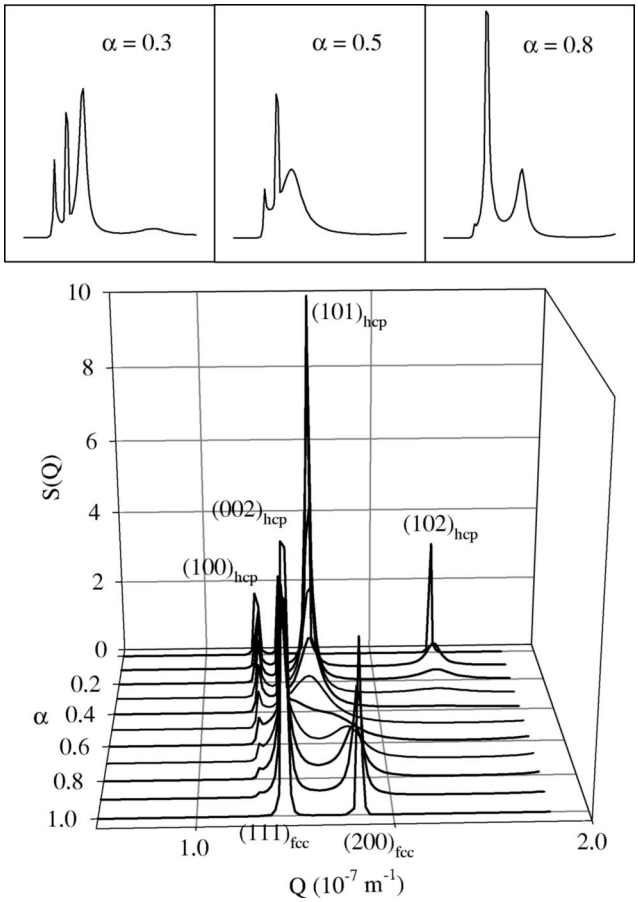

FIG. 3. Theoretical diffraction patterns for various stacking probabilities α.

IV. RESULTS

For orientationally invariant materials, such as fluids or crystal powders, consisting of monodisperse particles, the scattered intensity $I(Q)$ can be decomposed into $I(Q) \propto P(Q)S(Q)$ [34], where $P(Q)$ is the single-particle form factor and $S(Q)$ is the structure factor. When the system is polydisperse, however, this decomposition can no longer be done since the scattering amplitudes and positions are then correlated through their dependencies on the particles' radii. Nevertheless one can define a ''measured structure factor'' $S^M(Q)$ for a polydisperse system as the ratio of the intensity scattered by a concentrated suspension to that scattered by a dilute suspension, for which $S(Q)=1$ (particles' positions not correlated) [34].

The structure factors which we present in the following sections, although referred to as $S(Q)$, were obtained by measuring the intensity scattered by the concentrated suspensions $I(Q)$ and then dividing by the scattered intensity from dilute suspensions $I_{dil}(Q)$, measured in the exact same conditions as for the concentrated samples. They are all expressed in arbitrary units since we did not keep track of the exact concentrations of the dilute solutions nor of the exact scattering volumes, necessary for exact values $(S(Q) = (N_{dil}/N)[I(Q)/I(Q)_{dil}]$, where N and N_{dil} are the numbers of particles contained in the concentrated and dilute scattering volumes respectively). Typical measurements of $I(Q)$, $I_{dil}(Q)$ and resulting $S(Q)$ are plotted in Fig. 4.

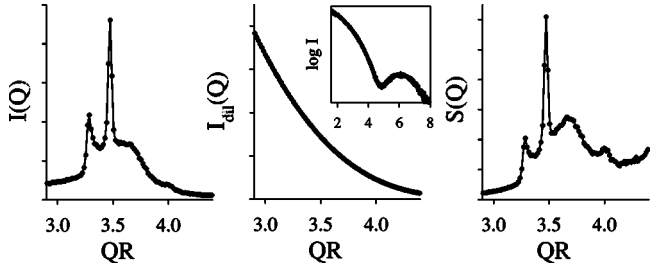

FIG. 4. Measured scattered intensities $I(Q)$, $I_{dil}(Q)$, and corresponding structure factor $S(Q)=I(Q)/I_{dil}(Q)$ (in arbitrary units).

A. Crystal structure after nucleation and growth

The effective hard-sphere volume fraction of the samples that we studied is 0.542, just below the melting volume fraction ϕ_M, where the samples are not quite fully crystalline and the crystal nucleation rate is near its maximum [35]. Each sample was initially homogenized to a metastable (quenched) fluid state by slow tumbling for several hours on a rotary mixer. It was then immediately placed in the sample holder of the light scattering setup (defining time $t=0$) and measurements of the scattered intensity $I(Q)$ collected at predetermined times (every 10–15 min) over a period of 3 h, until the crystallites had nucleated and grown. Figure 5 shows corresponding structure factors $S(Q)$ obtained for the sample in ''normal'' gravity (a) and that in reduced gravity (b). In both graphs, the lower curve corresponds to the metastable fluid, obtained immediately after shear melting ($t=0$), the middle curve to the first clear appearance of the Bragg reflection, and the upper curve to the ''end'' of the crystallization process. The measurements are virtually identical for both samples and therefore indicate the formation of similar crystalline structures. They show the appearance of a sharp Bragg reflection at $Q \approx 1.44 \times 10^7$ m^{-1} surrounded by a broad structured band of diffuse scattering. By reference to Fig. 3, one can observe the close resemblance of these newly emerged features with the predictions for a random hexagonal close-packed structure, with $\alpha \approx 0.5$.

In Fig. 6, these patterns are compared with theoretical ones. These were computed following the scheme outlined in Sec. III [33]. Three adjustable parameters were needed, an overall scaling factor, the average size of the crystallites and the stacking probability α. Powder averaging was carried out by numerical integration using Simpson's rule. Neither the exact shape of the crystals nor their exact size distribution proved to affect the patterns significantly; therefore, for simplicity, the crystals were assumed to be cubic and to have a Gaussian size distribution (width of 10%). Their average size was determined by fitting the width of the main Bragg peak to that of the peak of the experimental spectrum. Only the value of α significantly affects the shape of the powder pattern. It was iteratively adjusted so as to fit the experimental $S(Q)$ as well as possible. To account for the Brownian motion of the particles, thermal diffuse scattering was subtracted off the experimental data before fitting. We assumed a

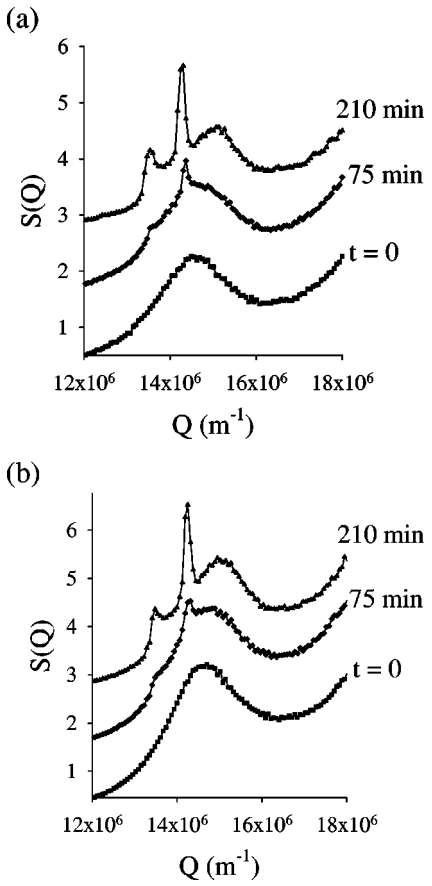

FIG. 5. Evolution of the structure factor $S(Q)$, during crystal nucleation and growth, for the system in normal gravity (a) and that in reduced gravity (b).

simple Einstein model, where each particle fluctuates independently about its own equilibrium position; under this asumption, the ''rigid-lattice'' structure factor $S(Q)$ can be derived from the measured structure factor $S_m(Q)$ via (see, e.g., [34])

$$S(Q)=e^{(1/3)Q^2\Delta r^2}[S_m(Q)+e^{-(1/3)Q^2\Delta r^2}-1], \qquad (1)$$

where Δr^2 is the mean-square random thermal displacement $\langle \Delta r_j{}^2 \rangle$; it was taken as 12% of the mean interparticle spacing [8]. Scattering from the coexisting fluid was also subtracted off the data prior to fitting; the fraction of fluid being small ($\approx 6\%$) we approximated its structure factor by that measured for the quenched fluid (time $t=0$).

As shown in Fig. 6, these patterns, measured immediately after crystal nucleation and growth are well described by purely random stacks of hexagonal layers, $\alpha=0.50$. In order to illustrate the sensitivity of the shape of the diffuse scattering to the value of α, we also show the calculated patterns for $\alpha=0.45$ and 0.55 (gray curves). Both the prepeak and the hump agree almost exactly with the calculations for $\alpha=0.50$. The slight disagreement between experiment and theory for small values of Q may be attributed to limitations of the Einstein model; in crystals the random thermal vibrations of the particles are clearly not independent, as assumed in our treatment. The discrepancy observed at higher Q is

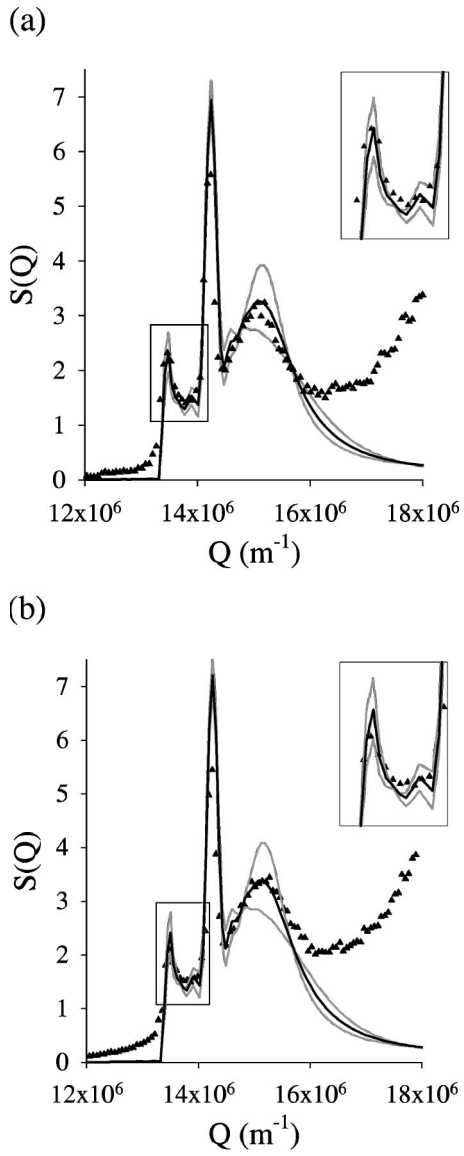

FIG. 6. Structure factors $S(Q)$, obtained immediately after crystal nucleation and growth, for the system in normal gravity (a) and that in reduced gravity (b) — after subtraction of the fluid scattering contribution and correction for the thermal motion of the particles (symbols). In both cases the data can be fitted by a random hexagonal close-packed pattern ($\alpha=0.50$), black line. To show the sensitivity of the diffuse scattering to the value of alpha, we have also plotted theoretical curves for $\alpha=0.45$ and $\alpha=0.55$, upper and lower gray lines, respectively. For all Q, the curve for $\alpha=0.50$ provides a much better fit to the data. The inset shows a closeup of the region of the prepeak. The increase in the measured data at high Q has no relation with the crystal structure; it is due to the proximity of the first minimum of the form factor.

due to the proximity of the first minimum of the form factor, which occurs near $Q=1.9\times10^7$ m^{-1} (Fig. 4). Because around this region the scattering is very weak, it may be corrupted by unwanted contributions, such as background scattering and residual multiple scattering, and it is therefore difficult to measure absolute values of $S(Q)$ for the corresponding wave vectors. Furthermore, this is a region where

even a small degree of polydispersity can affect the form of $S(Q)$. However, around $Q \sim 1.5 \times 10^7$ m^{-1}, close to the main peak of the structure factor and the region of most interest for the determination of the crystal structure, we expect polydispersity to have little effect on the structure factors. For (meta)stable fluidlike samples, where there is a correlation between particle size and position, a 5% polydispersity reduces the amplitude of the main peak slightly but hardly changes its shape (see, e.g., [34]). In a crystal, where average particle positions are set by the lattice, we expect a still smaller effect.

The structure of hard-sphere colloidal crystals, immediately after nucleation and growth, for sample concentrations just below melting, is therefore purely random hexagonal close packed, with a measured stacking probability $\alpha = 0.50 \pm 0.01$. Moreover, at this early stage, the crystal structure proves to be unaffected by the gravitational force imposed on the particles.

B. Aging of the structure

The powder patterns obtained on the same two samples, after being left undisturbed for one month, are shown in Figs. 7(a) and 7(b) for the sample in ''normal'' gravity and that in reduced gravity, respectively. The scattering pattern of the system in ''normal'' gravity has changed from that at early times. In particular, the features of the diffuse scattering around the main peak are not as pronounced; also noticeable, though quite small, is a new peak at $Q \approx 1.65 \times 10^7$ m^{-1}, which corresponds to the (200) line of an fcc structure. This new pattern can no longer be described by a single value of α. While the new shape of the diffuse scattering indicates a structure with $0.50 < \alpha \leqslant 0.60$, the presence of the $(200)_{fcc}$ peak is indicative of a crystalline structure much closer to pure fcc, i.e., $0.90 \leqslant \alpha \leqslant 1.0$. Indeed, the data can be well described by a coexistence of two different structures; the best fit is obtained for $98 \pm 1\%$, in volume, of faulty hexagonal close-packed crystals with $\alpha = 0.56$, and $2 \mp 1\%$ of pure fcc crystals ($\alpha = 1.0$); see Fig. 7(a). (We also tried other fits to the data, e.g., mixtures of two or three rhcp structures with different values of α. None of these gave significantly better results, so we quote here the model with the smallest number of adjustable parameters.)

The powder pattern of the system in reduced gravity, on the other hand, is almost identical to that at early times. The only difference is the slight growth of the $(200)_{fcc}$ reflection at $Q \approx 1.64 \times 10^7$ m^{-1}. It is well described by 98% of (nearly) random hexagonal close-packed crystals with $\alpha = 0.51$ and 2% of pure fcc crystals; see Fig. 7(b).

Thus there appears to be a correlation between the aging of the structure and the degree of gravity imposed on the particles. This shows in the evolution of the diffuse scattering band, which is the signature of the stacking disorder. While for the sample in reduced gravity, the features remained virtually unchanged over the 1 month duration of the experiment, a significant dampening of the diffuse scattering band was recorded for the sample in normal gravity, revealing an evolution of the random-stacked structure towards a slightly more fcc-like structure. The slight growth of the

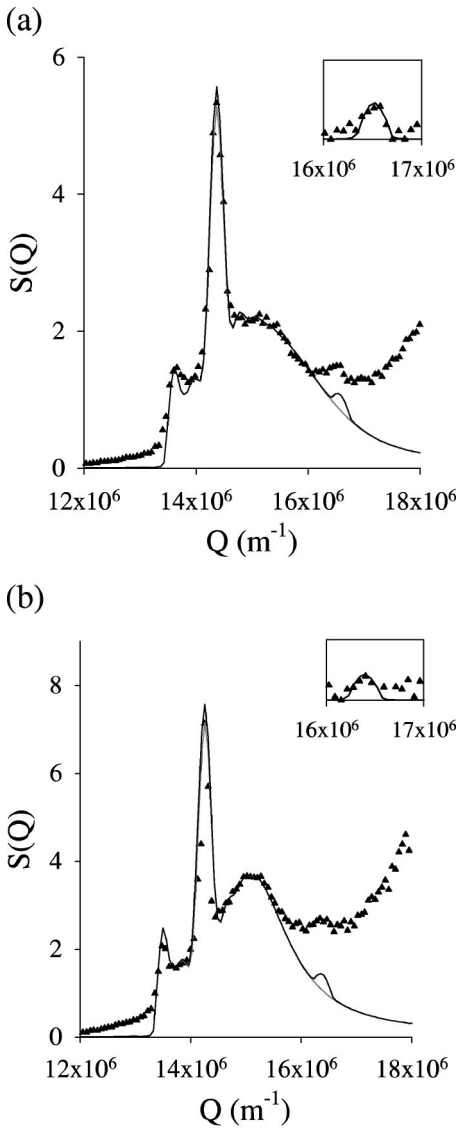

FIG. 7. Structure factors $S(Q)$ obtained on samples left undisturbed for 1 month after crystal nucleation and growth (symbols). The solid lines are theoretical fits. For the system in normal gravity (a), the experimental data points are fitted by a mixture of faulty hexagonal close-packed crystals with $\alpha = 0.56$, and a mean size of $N = 50$ layers across, and pure fcc crystals, with $\alpha = 1$ and $N = 30$, in the ratio 98:2. For the system in reduced gravity (b), the best fit corresponds to a mixture of (nearly) random hexagonal close-packed crystals with $\alpha = 0.51$, and a mean size $N = 50$, and pure fcc crystals, with $\alpha = 1$ and $N = 30$, in the ratio 98:2. The insets in the top right corners show the fits around the $(200)_{fcc}$ peak after subtraction of the baseline.

$(200)_{fcc}$ line, on the other hand, was almost equally observed for both samples, suggesting that it might not bear any relation to gravity.

C. Aging of the structure subjected to small perturbations

The same two samples showed substantially different results when handled during aging. The most striking difference was observed in the growth of the $(200)_{fcc}$ reflection,

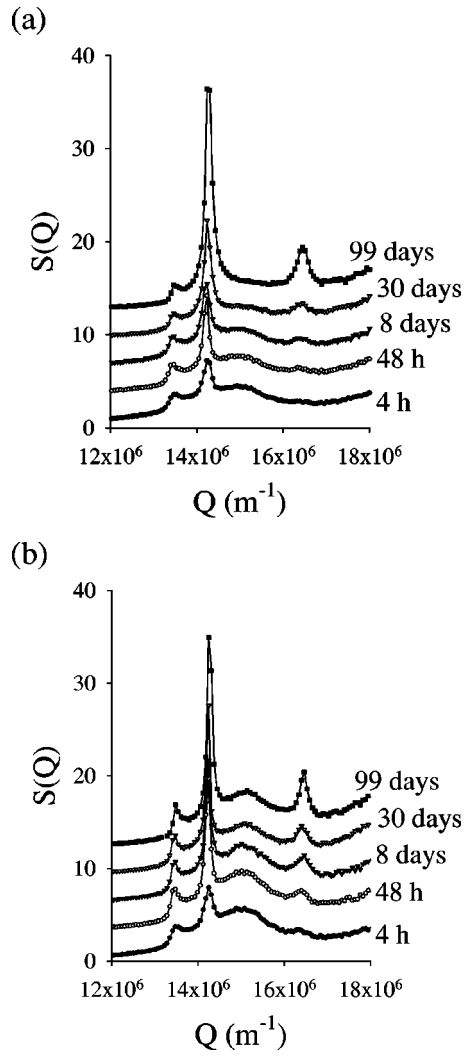

FIG. 8. Evolution of the structure factor $S(Q)$, after crystal nucleation and growth, for the system in normal gravity (a), and that in reduced gravity (b), subjected to small random perturbations (middle part of the samples).

which proved to be a lot more pronounced than for the samples left undisturbed. This is illustrated in Figs. 8(a) and 8(b), where we show results of periodic measurements performed on both samples (middle of sample cell) over a total period of three months starting after the initial homogeneous crystal nucleation. For each measurement the samples were manually transported from storage on a shelf to the light scattering equipment ($\approx$2 m away) and back. Although sample transportation was performed with utmost care (slow motion, smooth, with no sharp acceleration and minimum tilting), it is nevertheless obvious from the results that it affected the aging of the crystal structure. The difference in the size of the $(200)_{fcc}$ peak, in contrast with that obtained without moving the samples, is striking (cf. Fig. 7). The evolution of the rest of the patterns, on the other hand, remains in reasonably close agreement with the results obtained for the samples left undisturbed; the band of diffuse scattering exhibits pronounced features at early times for both samples (indicating a high degree of randomness) and gradually dampens out with time for the system in normal gravity (a), while for the system in reduced gravity (b) it remains virtually unchanged over the whole three-month period.

Again, by fitting theoretical curves to the data, we find that the patterns correspond to contributions from two types of close-packed arrangements. Figure 9 shows the fits calculated for the structure factors measured after 12 h, 1 month and 3 months on both samples. The results obtained after 12 h and 3 transits back and forth between storage and rig are very similar for the two samples. Analysis of the patterns shows a strong predominance of nearly random close-packed crystals, with $\alpha=0.52$ (95% in volume). The 5% volume content of pure fcc crystals is nevertheless higher than that measured on crystals aged for a whole month, when left undisturbed (Fig. 6), which therefore links the growth of the pure fcc component to those small perturbations inevitably imparted to the samples during transit. Measurements carried out after 1 month and 12 transits indicate that the amount of pure fcc crystals has increased even further, representing nearly 10% of the whole crystalline volume. After 3 months and 24 transportations, the volume fraction of fcc crystals has reached 14% in the sample in normal gravity and 12% in that in reduced gravity conditions. However, although the measured fraction of generated fcc crystals is virtually identical for both samples, the shape of the growing $(200)_{fcc}$ peak differs slightly between them; for the sample in normal gravity conditions, it indicates that the fraction of fcc crystals generated augments with time (and transits incurred) but that their mean size remains constant, while in reduced gravity conditions, the fcc crystals are also found to grow (cf. Fig. 9). The rest of the pattern also evolves in a somewhat different manner for the two samples but remains consistent with the results obtained on the samples unmoved. In the sample in normal gravity conditions, the large fraction of crystals which initially corresponds to a random hexagonal close-packed structure slowly evolves towards a more fcc-like ordering, with the stacking probability reaching a value of 0.6 after 3 months, while in the sample in reduced gravity, no significant evolution in the stacking probability is recorded over the time length of the experiment.

As stated earlier, measurements were performed at different heights in the samples. This was done essentially to assess the effect of gravity on the crystal structure. Owing to sedimentation, the samples evidenced the formation of several distinct layers over time [24]. In the sample in normal gravity, four different layers eventually formed, which, from top to bottom, consisted of a small region of clear supernatant, a small region of colloidal fluid, a larger region of polycrystalline solid, and finally a small high-density polycrystalline sediment. In the sample in reduced gravity, less sedimentation was observed and no clear supernatant was seen over the course of the three months; only three layers emerged, consisting of colloidal fluid, polycrystalline solid, and high-density polycrystalline sediment. The sedimentation rates being different in the two systems, the time scale over which these ''separations'' took place also varied greatly between the two samples. For each set of measurements, the positions of the sample and rectangular aperture were carefully readjusted so as to illuminate only the crys-

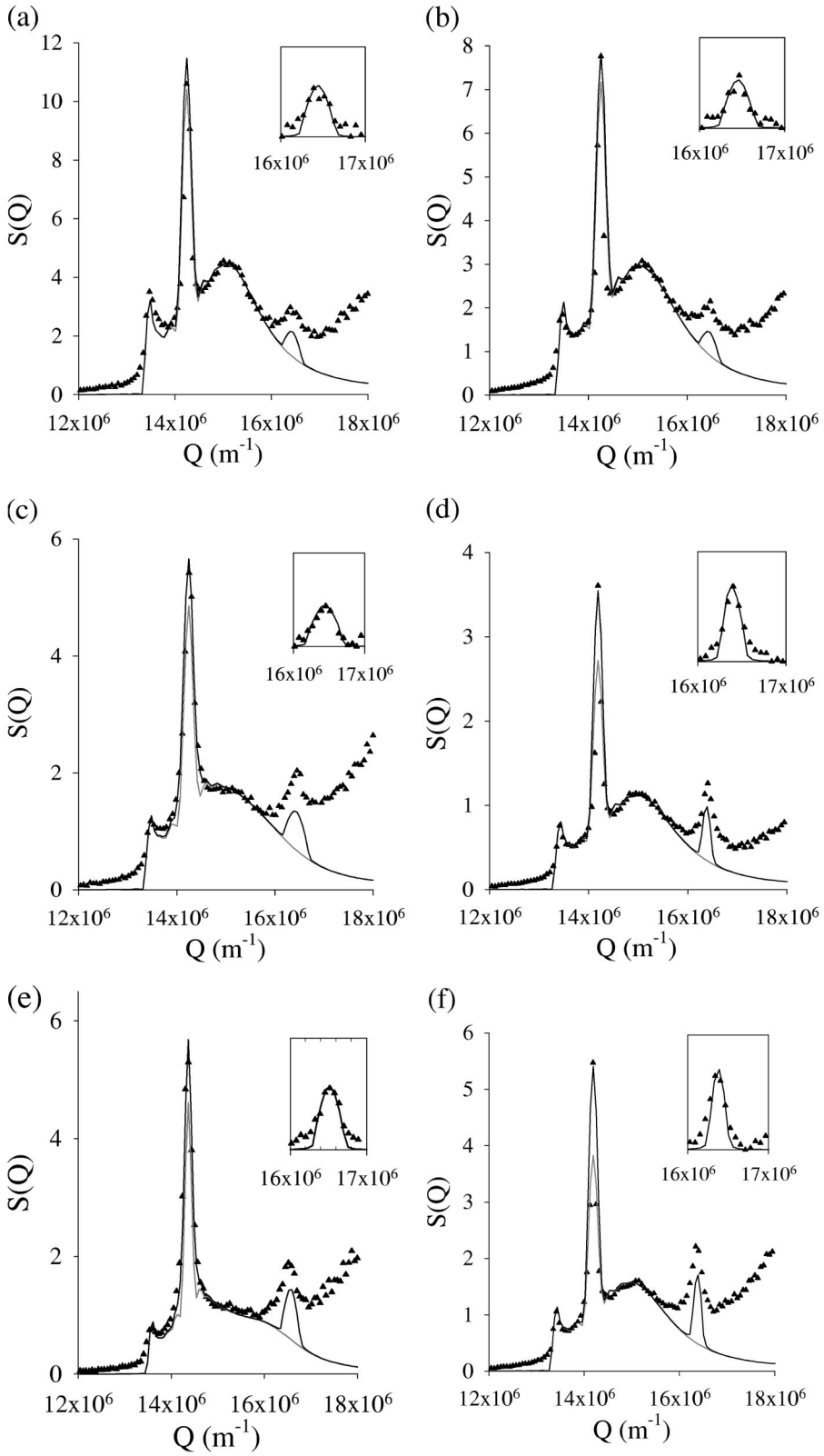

FIG. 9. Theoretical fits to the structure factors measured 12 hours, 1 month, and 3 months after crystal nucleation, on samples subjected to small random perturbations (manual transportation). (a) System in ''normal'' gravity after 12 hours and 3 transits between storage and rig; symbols are experimental data, line is theory corresponding to a mixture of (nearly) randomly stacked crystallites, with $\alpha=0.52$ and mean size $N=60$ layers across, and pure fcc crystallites, with $\alpha=1$ and $N=20$, in the ratio 95:5. (b) Same conditions as (a) for system in reduced gravity; best fit corresponds to a mixture of $\alpha=0.52$ ($N=60$) and $\alpha=1$ ($N=25$), in the ratio 95:5. (c) System in normal gravity after 1 month and 12 transits back and forth; theoretical fit corresponds to $\alpha=0.56$ ($N=70$) and $\alpha=1$ ($N=20$), in the ratio 90.5:9.5. (d) Same as (c) for system in reduced gravity; best fit corresponds to $\alpha=0.52$ ($N=60$) and $\alpha=1$ ($N=35$), in the ratio 91:9. (e) System in normal gravity after 3 months and 24 transportations back and forth; theory corresponds to $\alpha=0.6$ ($N=80$) and $\alpha=1$ ($N=20$), in the ratio 86:14. (f) Same as (e) for system in reduced gravity; theoretical fit corresponds to $\alpha=0.52$ ($N=60$) and $\alpha=1$ ($N=40$), in the ratio 88:12.

talline volume (divided into ten scattering slices). Most of the crystalline phase showed the trends plotted in Fig. 8. However, the very top and bottom parts were found to evolve quite differently from the main middle volume; the results for both samples are plotted in Fig. 10. Near the top [(a) and (b)], the growth of the $(200)_{fcc}$ reflection is more pronounced, indicating a higher proportion of the pure fcc component. The patterns measured after 3 months on both samples were fitted with theoretical ones; the results are shown in Fig. 11. We find that the amount of pure fcc crystals represents as much as $\approx 25\%$ of the total volume of the crystals sampled in the sample in normal gravity and nearly

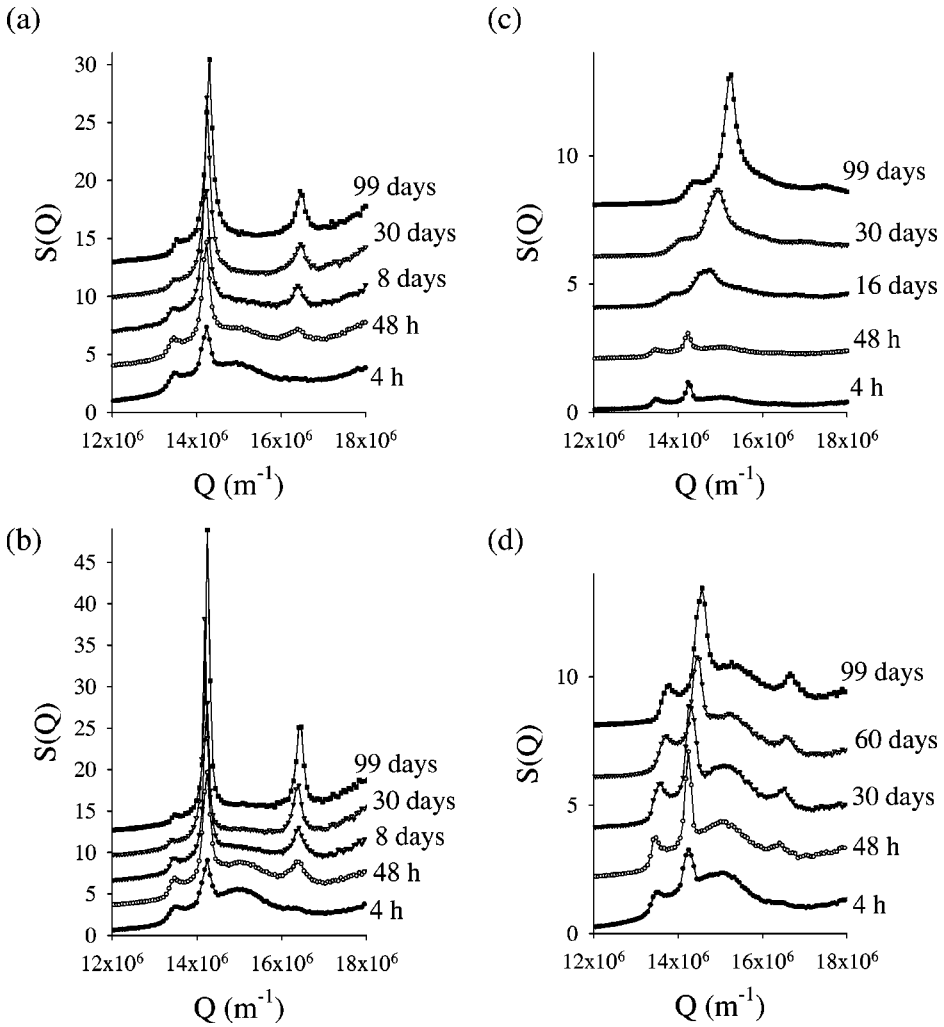

FIG. 10. Evolution of the structure factor $S(Q)$, after crystal nucleation and growth, in the top [(a) and (b), for the system in normal gravity and that in reduced gravity, respectively] and bottom [(c) and (d)] of the crystalline volumes, when subjected to small random perturbations.

40% in the sample in reduced gravity. This enhanced effect recorded near the top may be attributed to the fact that nearer the interface the perturbations incurred must be stronger.

Near the bottom of the container, the results are distinctly different and show the opposite trend, in that the $(200)_{fcc}$ peak is much less developped [Figs. 10(c) and 10(d)]. For the sample in normal gravity conditions, a significant shift of the pattern to higher Q values also indicates a decrease in the interlayer spacing, which can be explained by compaction of the crystals under gravity. Another noticeable difference is the broadening of the main peak, which implies a reduction in the size of the crystallites and could therefore mean that the crystals break under compression, melting somewhat at the grain boundaries; indeed, this is also indicated by the shape of the measured structure factor, after a week or so, showing the presence of some underlying fluid scattering superimposed on the crystal pattern. For the sample in reduced gravity, the measurements near the bottom of the container resemble more closely those recorded for the bulk crystals. The early patterns correspond to scattering contributions by rhcp and pure fcc crystals, and indicate a steady increase in the relative amount of fcc stacking. However, after a month, the shape of the pattern appears to ''freeze.'' Thereafter the only significant change is the slight shift of the curve to higher Q values. This again indicates a small decrease in the interlayer spacing, which must correspond to some compression of the crystals by the upper layers, under the effect of the excess gravitational forces. We may therefore speculate that the bottom crystals are less affected by the mechanical perturbations due to the confined geometry and the compression exerted by the upper crystallites (under gravity).

V. DISCUSSION

More than a decade ago Pusey *et al.* [16] showed that suspensions of colloidal hard spheres at concentrations near melting, when left to recrystallize undisturbed from the melt, initially formed purely random-stacked hexagonal close-packed structures. Our results (Fig. 6), for $\phi = 0.542$ (close to $\phi_M = 0.545$), are in excellent agreement with this early study and further show that the crystalline structure initially generated is unaffected by the strength of the gravitational force imposed on the particles. This new result also agrees with a study carried out at much the same time by Kegel and Dhont [22] for colloids in ''milligravity,'' as well as a more recent report by Cheng *et al.* [21] of measurements in a microgravity environment (on board the Space Shuttle Columbia).

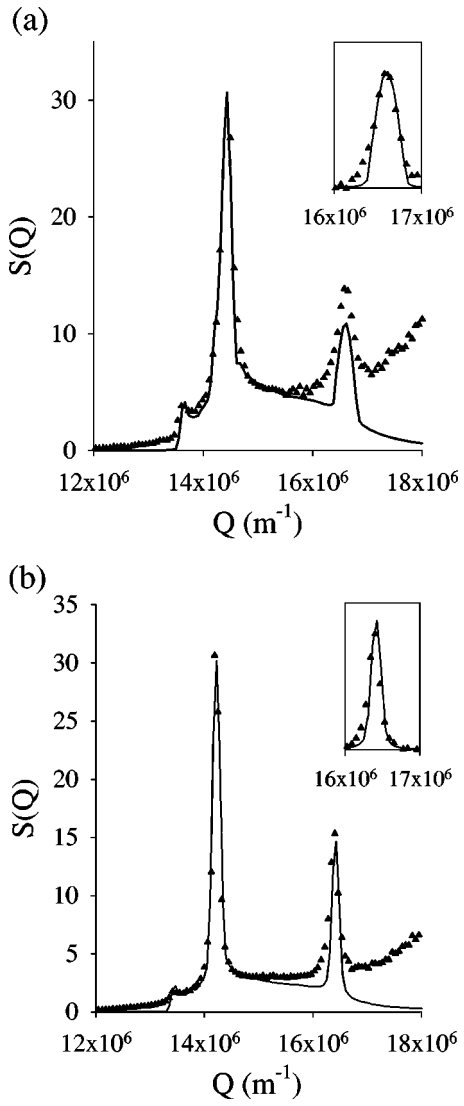

FIG. 11. Theoretical fits to the structure factors measured 3 months after crystal nucleation on the top crystal layers of samples subjected to small random perturbations. (a) System in ''normal'' gravity; symbols are experimental data, line is theory for a mixture of faulty stacked close-packed crystals with $\alpha=0.6$ ($N=80$) and of pure fcc crystals with $\alpha=1$ ($N=25$), in the ratio 75:25. (b) System in reduced gravity; best fit corresponds to a mixture of faulty stacked close-packed crystals with $\alpha=0.6$ ($N=80$) and of pure fcc crystals with $\alpha=1$ ($N=50$), in the ratio 61:39.

The main aim of this work, however, was to study the *aging* of these random-stacked structures, in the light of the new theoretical (computer simulation) results which have established fcc as the stable structure [12–15]. We have found that the crystalline structures are very sensitive to external perturbations. This is of significant importance for experiments since it implies that even very small mechanical perturbations must be considered. Our study shows that routine transfers, by hand, of the samples between storage on a shelf and the light scattering equipment, even when performed with utmost care, have a significant effect on the aging of the crystal structure. These ''random'' perturbations are found to encourage fcc stacking; pure fcc crystals are formed, as new crystals, while the remainder retain their original rhcp structure.

A. Spontaneous aging

In order to study any purely spontaneous aging of the colloidal crystals, one therefore has to leave the samples strictly undisturbed for the entire duration of the experiment. Under such conditions, however, we found only a small degree of aging of the structure over a period of one month. In both the normal- and the reduced-gravity samples, a few fcc crystals appeared, corresponding to about 2% of the total crystalline volume (Fig. 7). A second more noticeable change, discussed in Sec. V B (below), was found only in the system with particles subjected to high enough gravitational forces.

Pronk and Frenkel [13] recently estimated the rate at which rhcp crystals are expected to convert into pure fcc crystals. Their treatment assumes that the fcc crystals grow at the grain boundaries and ignores bulk rearrangement as well as shear-induced restacking. Using a Wilson-Frenkel growth law, they arrive at a velocity of the fcc crystal front v_{cr} approximated by

$$v_{cr}=\frac{\zeta D}{\Lambda}[\exp(\Delta f/k_BT)-1], \tag{2}$$

where Δf is the magnitude of the free-energy difference per particle between the rhcp phase and the stable fcc phase, D is the (short-time) self-diffusion constant in the dense colloidal suspension, Λ is a characteristic distance over which a particle should diffuse in order to be incorporated in the fcc crystal, which, assuming the grain boundaries to be liquid-like, they take to be of the order of the particle diameter, and ζ is a (dimensionless) proportionality factor of order unity. The resulting estimate for v_{cr} in our case is $v_{cr}\approx 5\times10^{-11}$ m s^{-1}, where we have taken $\Delta f\approx 6\times10^{-4}k_BT$ [13] and $D\approx 4\times10^{-14}$ m^2 s^{-1} [36]. A rough comparison with this prediction can be made by estimating the spontaneous rate of conversion in our system from the results obtained in unperturbed conditions (cf. Fig. 7). This can be done based on the fraction of fcc crystals formed over time; our results showed that after 1 month the fraction of fcc represented $\approx 2\%$ of the total crystalline volume, which indicates a rate of growth of the fcc front of the order of $v_{cr}\approx 3\times10^{-12}$ m s^{-1}. Alternatively, v_{cr} can be estimated from the average size L of the fcc crystals after 1 month; we found $L\approx 30$ particles across, which gives $v_{cr}\approx 6\times10^{-12}$ m s^{-1}. The slight disagreement between these two estimates may simply be attributed to the different approximations/assumptions made; e.g. in the first case, the fcc crystallites are modeled as thin slabs growing on the faces of the rhcp crystals, while in the second case, they are assumed to have cubic shapes (assumption made in the theoretical model used to fit the data). Direct comparison with the theoretical estimate indicates that the conversion to fcc occurs ≈ 10 times slower in our experiments than predicted. However, as discussed by Pronk and Frenkel [13], the exact rate of restacking depends sensitively on the size distribution of the crys-

tals. Proper comparison with their predictions would therefore require more knowledge of the transformations than those available by performing only scattering experiments. It is also possible that a more complete theory would predict a value of the factor ζ smaller than 1.

B. Aging induced by gravity

In the sample subjected to normal gravity, a second change, in addition to the growth of a few fcc crystals, was observed when it was left undisturbed for one month. It corresponded to a slow rearrangement, apparently in the bulk of the crystals, of the initial rhcp structure towards a more fcc-like stacking, with the stacking probability α changing from 0.50 to 0.56 over the month [Fig. 7(a)]. Thus this indicates that fcc stacking is also favored by gravity-induced stresses. However, the ripening towards fcc due to gravity differs markedly from the perturbation-induced transformations, where discrete regions of pure fcc order are created, and instead consists of an overall rearrangement of the original rhcp crystals towards a more fcc-like order. Perhaps this rearrangement is associated with the slow flow of the suspension medium through the crystals as they settle. The exact mechanism remains to be established.

C. Aging caused by mechanical perturbations

When the samples were transferred by hand from storage to the light scattering equipment they were inevitably subjected to small degrees of tilting and rotation. The colloidal crystals are extremely weak mechanically, so that such motions are likely to cause small shear flows within the samples which themselves cause some ''shear melting'' of the crystals, probably mainly at grain boundaries. It is possible that these shear-melted regions then regrew as predominantly fcc.

It is difficult to calculate the strength of these effects; one can only get an order of magnitude. Let us first consider the stresses exerted by tilting the sample. We can estimate a strain of the order of $\gamma \approx 10^{-1}$ which, applied at a frequency $\nu \approx 0.5$ Hz, corresponds to a strain rate $\dot{\gamma} \approx 5 \times 10^{-2}$ Hz. Assuming a Newtonian behavior, which is reasonable at low shear, the shear stress can then be calculated from $\sigma_t = \eta \dot{\gamma}$, where η is the viscosity of the suspension, $\eta \approx 3 \times 10^{-1}$ N m^{-2} s [37]. We therefore estimate the shear stress, due to tilting of the sample, of the order of $\sigma_t \approx 10^{-2}$ N m^{-2}. Let us now consider the shear stress applied by rotating the sample. A very rough estimate can be obtained by assuming a viscous laminar flow and stick boundary conditions. Assuming a shear rate of the order of $\dot{\gamma} \approx 10^{-1}$ Hz, we obtain a shear stress of the order of $\sigma_r \approx 10^{-2}$ N m^{-2}, and therefore of similar magnitude. But how do these values compare with the yield stress of the crystallites? The yield stress, σ_y, for colloidal crystals is typically a few percent of their elastic shear modulus G; for $G \approx 1$ N m^{-2} [38] we get $\sigma_y \approx 10^{-2}$ N m^{-2}. The yield stress of the crystallites therefore appears to be of the same magnitude as the shear stresses inadvertantly imparted by transport, which supports the hypothesis of some ''shear melting'' of the crystals.

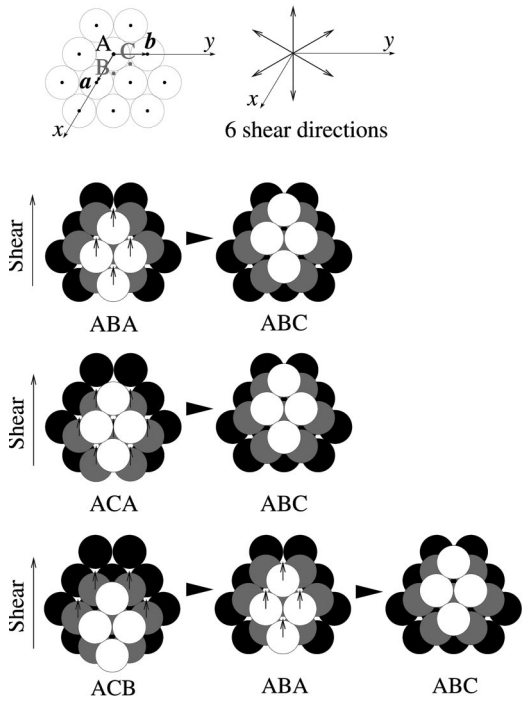

FIG. 12. Effect of small shears applied to close-packed structures, illustrated on a stack of three layers. Shear applied along any of the six directions indicated in the top right of the figure can allow layers to slide over/past each other. Whether a layer can slide depends on the local stacking order. However, the resulting shear-induced order is always fcc, irrespective of the initial stacking.

To try to obtain a clearer understanding of these processes, we also studied the structural response of the early rhcp crystals to controlled rocking and rotational motions (about the vertical axis). Samples subjected to rocking motions alone showed the presence of pure fcc crystals but only near the top where macroscopic flow was induced and not throughout the sample as was found with the ''random'' perturbations. Rotational motions alone had no significant effect on any part of the crystalline volume. However, combinations of the two types of motions applied simultaneously proved to have a very similar effect to that of the random perturbations. No careful experiment was actually performed that combined the two motions but preliminary results evidenced the formation of a growing fraction of pure fcc crystals throughout the sample.

In fact, using a simple argument, it is easy to see how small shears applied to any arbitrary stack of close-packed layers can be expected to favor fcc order. This is illustrated in Fig. 12, on a stack of three hexagonal close-packed layers with a shear applied along one of the six directions defined by the vectors $\boldsymbol{a}/3+2\boldsymbol{b}/3$ and $2\boldsymbol{a}/3+\boldsymbol{b}/3$ and, for reason of symmetry, those obtained by rotation of 120° in both directions (where $\boldsymbol{a}$ and $\boldsymbol{b}$ are hexagonal lattice vectors in layers); we may assume that small shears applied in the other directions have no significant effect. According to its registered position, each layer can either slide along to the next allowed position in the direction of the applied shear, or remain in its current position if jammed up against the particles in the neighboring layers. As shown in Fig. 12, where the bottom

layer is assumed fixed (e.g., jammed up against the particles in the layer underneath), once the two other layers have been forced to move along to new accessible positions in the direction of the shear until jammed, the resulting order is fcc whatever the initial stacking order. This is also true for any of the six shear directions mentioned above.

Presumably, in view of theoretical predictions that the fcc structure of hard spheres has the lowest free energy [12–15], the fcc crystals induced by this shearing mechanism must be regarded as stable.

D. Comparison with other experiments

While it is now theoretically well established that fcc is the stable structure of crystals of hard spheres [12–15], the literature on experimental aging towards fcc is rather confused [16–22]. However, by showing how sensitive the colloidal crystals are to the exact experimental conditions, our study may have helped to resolve the grounds underlying these discrepancies. While experimental conditions have always been treated as a crucial factor in the nucleation of colloidal crystals, they appear to have been more or less neglected when studying aging of the crystal structures. The first report of a ripening of rhcp towards fcc in colloidal hard spheres, by Chui [17], was based on a similar light scattering study to the one reported here for a system also very similar to ours in ''normal'' gravity, and therefore can be directly compared with our results. Their observations revealed the formation of a significant fraction of fcc crystals within merely 1 week, by far exceeding that measured in our sample after a whole month in perturbation-free conditions. However, the evolution of their measured powder pattern (Fig. 8 in [18]) coincides conspicuously with our measurements for the sample subjected to repeated manual transportations between storage and rig [Fig. 9(a)], where the fraction of fcc crystals generated after 1 month amounts to ≈ 5 times that measured in the sample left undisturbed during the same length of time. This strongly suggests therefore that the reported ripening was also induced by external disturbances, a fact which was simply overlooked at the time.

More recently, Kegel and Dhont [22] also reported light scattering measurements of hard-sphere crystals at similar volume fraction ($\phi = 0.55$) which again show the emergence of the fcc (200) feature sooner than we found here (Fig. 1 in [22]). The system they studied differs from ours in several respects; the colloidal particles are about twice as large as the ones studied here, and the suspension medium is a different mixture of solvents with a viscosity η roughly half that of our mixtures. Since the Brownian time τ varies as $\tau \sim \eta R^3$, the dynamic evolution of their system is actually expected to be roughly 4 times slower than that of the one studied here (the Brownian time is the time $\tau \sim R^2/D$ taken by a particle to diffuse a distance equal to its radius). Another difference between the two systems is in the gravitational length $h = k_B T/m_B g$ (where m_B is the particles' buoyant mass). Not only is h greater in their system (roughly 10 times larger than that in our reduced gravity system) so that gravitational stresses are smaller, but our results also indicate that gravity-induced stresses do not generate pure fcc crystals but instead cause an overall rearrangement of the stacking towards fcc. In fact, although the authors explicitly specify that perturbation-free conditions were ensured during crystal nucleation, they do not mention any such precautions undertaken thereafter, during aging. We therefore wonder whether the accelerated growth of fcc crystals reported in this study results from ''random'' perturbations applied during aging, for example by moving the samples.

One last point that merits further comment is the effect of the gravitational stresses on the crystal structure. The role of gravity was first questioned by Zhu *et al.* [19]. From their observations on crystals in microgravity, showing the absence of fcc growth, they concluded that gravity-induced stresses were at the origin of the ripening towards fcc reported for samples in normal gravity. This conclusion was also supported by Kegel and Dhont for the results discussed above. However, in a recent publication by Cheng *et al.* [21], data collected in the same microgravity conditions now show the gradual growth of fcc crystals in samples at various volume fractions (in and above the coexistence region). Although the earlier results suffered a lower resolution of scattering angle than the later ones, this disagreement appears rather conspicuous. Furthermore, the new report shows very fast rates of fcc growth. This is all the more surprising since the colloidal particles used are relatively large (lower D). We are again prompted to question the possible mediation by external perturbations.

So, is the crystal structure affected by gravitational stress? Our study reveals that it is; as shown in Fig. 7(a) for perturbation-free conditions, the evolution of the powder pattern indicates a rearrangement of the initial rhcp structure towards a more fcc-like stacking. This rearrangement is very slow and differs distinctly from the ''aging'' observed under small mechanical perturbations.

VI. CONCLUSION

Our results demonstrate how very small mechanical perturbations applied to hard-sphere colloidal crystals can significantly affect the aging of their structure: they appear to shear-melt a fraction of the rhcp crystals, allowing them to regrow as almost pure fcc. Previous reports, which failed to identify this crucial effect/factor, have contributed to a rather confused literature on this topic and can now be looked at in a new light. When the samples are left unperturbed, we find that, as predicted by Pronk and Frenkel [13], the spontaneous aging of the initial rhcp structure towards fcc is very slow. We also observe a slow rearrangement of the random stacking towards a more fcc-like stacking under gravity, probably driven by the hydrodynamic flow through the crystals.

ACKNOWLEDGMENTS

The work reported here was partly funded by the U.K. Engineering and Physical Sciences Research Council. We thank S. I. Henderson and P. Bartlett for kindly providing the powder diffraction code. We also acknowledge valuable discussions with A. D. Bruce, G. J. Ackland, and A. N. Jackson.

[1] W.W. Wood and J.D. Jacobson, J. Chem. Phys. **27**, 1207 (1957).
[2] B.J. Alder and T.E. Wainwright, J. Chem. Phys. **27**, 1208 (1957).
[3] J. Kepler, *Strena, The Six-Cornered Snowflake* (Tampach, Frankfurt, 1611).
[4] T.C. Hales, Discrete Comput. Geom. **17**, 1 (1997).
[5] T.C. Hales, Discrete Comput. Geom. **18**, 135 (1997).
[6] B.J. Alder, W.G. Hoover, and D.A. Young, J. Chem. Phys. **49**, 3688 (1968).
[7] B.J. Alder, B.P. Carter, and D.A. Young, Phys. Rev. **183**, 831 (1969).
[8] D.A. Young and B.J. Alder, J. Chem. Phys. **60**, 1254 (1974).
[9] D. Frenkel and A.J.C. Ladd, J. Chem. Phys. **81**, 3188 (1984).
[10] J.L. Colot and M. Baus, Mol. Phys. **56**, 807 (1985).
[11] F. Iglói, J. Phys. C **19**, 6907 (1986).
[12] P.G. Bolhuis, D. Frenkel, S.-C. Mau, and D.A. Huse, Nature (London) **388**, 235 (1997).
[13] S. Pronk and D. Frenkel, J. Chem. Phys. **110**, 4589 (1999).
[14] S.-C. Mau and D.A. Huse, Phys. Rev. E **59**, 4396 (1999).
[15] A.D. Bruce, A.N. Jackson, G.J. Ackland, and N.B. Wilding, Phys. Rev. E **61**, 906 (2000).
[16] P.N. Pusey, W. van Megen, P. Bartlett, B.J. Ackerson, J.G. Rarity, and S.M. Underwood, Phys. Rev. Lett. **63**, 2753 (1989).
[17] T. T. Chui, M. Phil. thesis, The University of Edinburgh, 1994; see also Ref. [18].
[18] W. C. K. Poon and P. N. Pusey, in *Observation, Prediction and Simulation of Phase Transitions in Complex Fluids*, edited by M. Baus *et al.* (Kluwer Academic, Dordrecht, 1995), pp. 3–51.
[19] J. Zhu, M. Li, R. Rogers, W. Meyer, R.H. Ottewill, STS-73 Space Shuttle Crew, W.B. Russel, and P.M. Chaikin, Nature (London) **387**, 883 (1997).
[20] W.B. Russel, P.M. Chaikin, J. Zhu, W.V. Meyer, and R. Rogers, Langmuir **13**, 3871 (1997).
[21] Z. Cheng, J. Zhu, W.B. Russel, W.V. Meyer, and P.M. Chaikin, Appl. Opt. **40**, 4146 (2001).
[22] W.K. Kegel and J.K.G. Dhont, J. Chem. Phys. **112**, 3431 (2000).
[23] L. Antl, J.W. Goodwin, R.D. Hill, R.H. Ottewill, S.M. Owens, S. Papworth, and J.A. Waters, Colloids Surf. **17**, 67 (1986).
[24] S.E. Paulin and B.J. Ackerson, Phys. Rev. Lett. **64**, 2663 (1990).
[25] S.M. Clarke, R.H. Ottewill, and A.R. Rennie, Adv. Colloid Interface Sci. **60**, 95 (1995).
[26] P.N. Pusey and W. van Megen, J. Chem. Phys. **80**, 3513 (1984).
[27] A. Moussaïd and P.N. Pusey, Phys. Rev. E **60**, 5670 (1999).
[28] S.-E. Phan, W.B. Russel, Z. Cheng, J. Zhu, P.M. Chaikin, J.H. Dunsmuir, and R.H. Ottewill, Phys. Rev. E **54**, 6633 (1996).
[29] P.N. Pusey and W. van Megen, Nature (London) **320**, 340 (1986).
[30] W.G. Hoover and F.H. Ree, J. Chem. Phys. **49**, 3609 (1968).
[31] A. Guinier, *X-Ray Diffraction* (Freeman, New York, 1963).
[32] W. Loose and B.J. Ackerson, J. Chem. Phys. **101**, 7211 (1994).
[33] S. I. Henderson, POLYXTAL Turbo-Pascal code, 1995.
[34] P. N. Pusey, in *Liquids, Freezing and Glass Transition*, edited by J. P. Hansen, D. Levesque, and J. Zinn-Justin (Elsevier, Amsterdam, 1991), pp. 763–942.
[35] J.L. Harland and W. van Megen, Phys. Rev. E **55**, 3054 (1997).
[36] W. van Megen, T.C. Mortensen, S.R. Williams, and J. Müller, Phys. Rev. E **58**, 6073 (1998).
[37] S.P. Meeker, W.C.K. Poon, and P.N. Pusey, Phys. Rev. E **55**, 5718 (1997).
[38] S.E. Phan, M. Li, W.B. Russel, J.X. Zhu, P.M. Chaikin, and C.T. Lant, Phys. Rev. E **60**, 1988 (1999).